Journal of Controlled Release 140 (2009) 100–107

Contents lists available at ScienceDirect

Journal of Controlled Release

journal homepage: www.elsevier.com/locate/jconrel

Dual targeting improves microbubble contrast agent adhesion to VCAM-1 and P-selectin under flow

E.A. Ferrante [a,*], J.E. Pickard [a], J. Rychak [b], A. Klibanov [c], K. Ley [d]

[a] Department of Biomedical Engineering, University of Virginia, Charlottesville, VA 22908, USA
[b] Robert M. Berne Cardiovascular Research Center, University of Virginia, Charlottesville, VA 22908, USA
[c] Department of Medicine, University of Virginia, Charlottesville, VA 22908, USA
[d] La Jolla Institute of Allergy and Immunology, La Jolla, CA 92037, USA

ARTICLE INFO

Article history:
Received 9 January 2009
Accepted 1 August 2009
Available online 8 August 2009

Keywords:
Ultrasound contrast
Targeting
Microbubbles
P-selectin
VCAM-1

ABSTRACT

To improve ultrasound contrast agents targeted to the adhesion molecules P-selectin and VCAM-1 for the purpose of molecular imaging of atherosclerotic plaques, perfluorocarbon-filled phospholipid microbubble contrast agents were coupled by a polyethylene glycol–biotin–streptavidin bridge with mAb MVCAM.A (429), a sialyl Lewis^x polymer (PAA-sLe^x), or both (dual). Approximately three hundred thousand antibody molecules were coupled to the surface of each microbubble. Recombinant mouse P-selectin and/or VCAM-1 coated on flow chambers showed saturation of binding at approximately 15 ng/μl, resulting in 800 and 1200 molecules/μm^2 for P-selectin and VCAM-1, respectively. Dual substrates coated with equal concentrations of P-selectin and VCAM-1 had site densities between 50 and 60% of single substrates. When microbubbles were perfused through flow chambers at 5×10^6 microbubbles/ml (wall shear stress from 1.5 to 6 dyn/cm^2) dual-targeted microbubbles adhered almost twice as efficiently as single-targeted microbubbles at 6 dyn/cm^2. The present study suggests that dual-targeted contrast agents may be useful for atherosclerotic plaque detection at physiologically relevant shear stresses.

1. Introduction

Coronary heart disease, a large portion of which is attributable to atherosclerosis, is the leading cause of deaths in the United States, claiming a total of 452,300 lives in 2004 as reported by the American Heart Association [1] and the Centers for Disease Control. Vascular inflammation contributes to atherosclerotic plaque formation and progression. Within athero-prone regions of the vasculature, activated endothelial cells express pro-inflammatory surface molecules such as selectins (E- and P-selectin) that promote rolling of leukocytes on the blood vessel surface and immunoglobulin superfamily members (ICAM-1, VCAM-1) that support firm adhesion and migration of leukocytes into the tissue [2].

Most selectin interactions are mediated by P-selectin glycoprotein ligand 1 (PSGL-1), expressed by monocytes and neutrophils [3,4]. Selectin binding is characterized by a high on-rate and off-rate [5] to promote leukocyte capture under flow and subsequent rolling. Firm monocyte adhesion and arrest, on the other hand, are mediated mostly by interactions between VCAM-1 and $\alpha_4\beta_1$ integrin [2].

In atherosclerosis, early types of lesions (types I, II, III and IV) [6,7] are difficult to detect and are often termed "silent" plaques because the individuals affected are generally asymptomatic. At the advanced stages of the disease, a "vulnerable" plaque is characterized by a large lipid pool with a necrotic core within the intima, large amounts of macrophages that express thrombogenic factors and a thin, collagen-poor fibrous cap but no stenosis of the blood vessel lumen [8,9]. Many vulnerable atherosclerotic lesions remain undetected until a severe event, such as plaque rupture and thrombosis, occurs, and no method exists to reliably detect inflamed "vulnerable" atherosclerotic plaques.

In molecular imaging, the use of imaging agents enhances the contrast between different types of tissue within the body, providing integrated information between molecular level events and the physiological environment in which they take place [10,11]. The use of biomarkers that can specifically target and elucidate molecular level interactions within the body not only aids to further the understanding of how biological processes work but also increases the chances of earlier disease detection. Although microbubbles have been used as ultrasound contrast agents to enhance the weak echo signals generated by the blood pool for several decades [12], in molecular imaging they have further potential of being used to target specific areas of blood vessels to indicate the onset of disease states [13–15].

The targeted ultrasound contrast system investigated for this project consisted of perfluorocarbon-filled microbubbles with a poly (ethylene glycol) (PEG)-phospholipid shell. The PEG shell forms a short brush to enhance microbubble stability, while longer PEG

* Corresponding author. Robert M. Berne Cardiovascular Research Center, University of Virginia, 415 Lane Road, Charlottesville, VA 22908, USA. Tel.: +1 434 825 4616.
E-mail address: eaf4z@virginia.edu (E.A. Ferrante).

0168-3659/$ – see front matter © 2009 Elsevier B.V. All rights reserved.
doi:10.1016/j.jconrel.2009.08.001

tethers interdispersed around the microbubble provides sites for antibody or carbohydrate attachment. This ultrasound contrast agent system is modeled based on the behavior of leukocytes during inflammation, which use ligands to P-selectin and VCAM-1 to roll and eventually attach to the blood vessel wall [2,5]. We used a monoclonal antibody to VCAM-1, MVCAM.A(429) and a synthetic polymeric sLe^x (PAA-sLe^x) with affinity to P-selectin [16,17] to mediate capture and rolling interactions between microbubbles and the target substrate.

The surface coverage of targeting ligands on the microbubble determines the ratios of targeting ligands that can best promote maximal attachment of microbubbles with the appropriate balance of rolling and arrest interactions. The site densities of target molecules adsorbed to the surface of flow chambers modulates the response of molecularly targeted microbubbles in a controlled flow environment designed to mimic temporally and spatially the in vivo expression of pro-inflammatory molecules on activated endothelium. The attachment performance of these ultrasound contrast agents varies depending on the fluid shear stress levels that they experience when being delivered to a target substrate, as well as on the microbubble and substrate molecular composition and site densities.

In this study, radioiodinated antibodies against VCAM-1 and P-selectin were used to probe the site densities of proteins adsorbed to polystyrene flow chamber substrates. The number of antibody molecules attached to the surface of single- and dual-targeted microbubbles was probed using fluorescently-labeled antibodies in combination with flow cytometry and a set of calibration standards. A parallel plate flow chamber under transillumination was used to determine the adhesion efficiency of dual-targeted microbubbles as compared to their single-targeted counterparts at various levels of fluid wall shear stress, laying the groundwork for the development of a well-characterized and efficient ultrasound-based molecular imaging system for the detection of atherosclerotic plaques.

2. Methods

2.1. Iodination of antibodies and substrate preparation

Monoclonal antibodies MVCAM.A(429) [18] (Pharmingen; San Diego, CA) and Rb40.34 [19,20] (Lymphocyte Culture Center; University of Virginia, VA) were radioactively labeled with $Na^{125}I$ (PerkinElmer Wallac; Turku, Finland) using Iodogen pre-coated iodination tubes (Pierce; Rockford, IL). Briefly, upon hydration of an iodination tube with Tris buffer (25 mM of Tris–HCl, pH 7.5, 0.4 M NaCl), the iodination reagent (1,3,4,6-tetrachloro-3α,6α-diphenylglycouril) was added and incubated to an aliquot of antibody for 6 min at room temperature, mixing every 30 s. Excess $Na^{125}I$ was quenched with 50 μl of scavenging buffer (10 mg/ml of tyrosine in Tris iodination buffer). The radiolabeled antibody was desalted with D-Salt™ Polyacrylamide desalting column (6K MWCO, Pierce) which was used to increase protein recovery and the radioactivity of the recovered samples was measured by a Wallac 1470 gamma counter (PerkinElmer Wallac). Antibody concentration was measured with a Coomassie Plus protein assay (Pierce; Rockford, IL) with a spectrophotometer at 595 nm. Values from these measurements were used to obtain specific activity (CPM/μl). Isotype control antibodies for Rb40.34 (IgG_1, R3-34; Pharmingen; San Diego, CA) and MVCAM.A (429) (IgG_{2a}, R35-95; Pharmingen; San Diego, CA) were radiolabeled in the same manner.

The flow chamber Petri dish (35 mm, Corning Inc.; Corning, NY) was incubated with VCAM-1.Fc, P-selectin.Fc (R&D Systems; Minneapolis, MN) or both diluted to the desired concentration in 200 μl of PBS overnight at 4 °C and covered with a plastic 22×22 mm cover slip (Fisher Scientific; Pittsburg, PA). Substrates were then washed with a 1% Tween/Ultrapure water solution and blocked against non-specific interactions with casein in TBS (Pierce) for 2 h at 4 °C prior to use. Control substrates were incubated with casein alone.

2.2. Site density measurements

P-selectin and/or VCAM-1 were coated with 0, 0.5, 1, 2, 4, 8, 16 and 30 ng/μl of protein in PBS. Substrates were incubated with approximately 3 μg of radioactive antibody for 30 min, washed twice with PBS and incubated with 0.1 M NaOH/5% SDS for 10 min at room temperature. The radioactivity of this solution was measured with a gamma counter (PerkinElmer Wallac; Turku, Finland) to account for losses in activity from day to day. I^{125} has a 60 day half-life and all experiments were completed within days of antibody iodination. Combined with the concentration measurement for the antibody stock, this was used to determine the amount of radiolabeled antibody bound to the surface of each plate. Radioactively labeled isotype antibodies were used to determine the specificity of MVCAM.A(429) and Rb40.34 against VCAM-1 and P-selectin, respectively.

The Langmuir–Freundlich isotherm for protein adsorption [21] was used to fit all protein adsorption results. This isotherm is given by $B = \frac{B_{max} * F^n}{K_a + F^n}$, where B corresponds to bound molecules/μm^2, F denotes the free molecules available for binding, B_{max} is the maximum binding capacity, K_a denotes the adsorption constant for the protein and n is the Langmuir–Freundlich parameter. Curve fitting parameters for each of the data curves shown were obtained by using the MATLAB (The MathWorks; Natick, NA) curve fitting tool (cftool). The r^2 values for all curves were approximately 0.99. The table below shows the values obtained for the isotherm constants.

	VCAM-1, single substrates	P-selectin, single substrates	VCAM-1, dual substrates	P-selectin, dual substrates
n	1.918	1.837	2.039	1.735
B_{max}	1461	809	867	519.2
K_a	45.62	13.49	159.1	41.49

2.3. Targeting molecules and microbubble preparation

Biotinylated MVCAM.A(429) was conjugated to Alexa Fluor 647 using a labeling kit (Molecular Probes, Eugene, OR). Briefly, 100 μg of unconjugated antibody was incubated with a pre-measured amount of Alexa Flour 647 reactive dye for 1 h at room temperature and then overnight at 4 °C. After conjugation, excess unbound fluorochrome was removed by centrifugation in a 5 kDa MW cut-off Amicon tube (Millipore; Billerica, MA) for 20 min at 5000g until free dye in the supernatant was no longer detected. Using a spectrophotometer, the concentration and degree of labeling were measured by reading the absorbance of the sample at 280 and 650 nm. Absorbance measurements at a wavelength of 280 nm allow the determination of the concentration of the antibody in a solution, while absorbance measurements at 650 nm allow the determination of the degree of fluorescence labeling (for Alexa Fluor 647) achieved per antibody molecule. Absorbance measurements were converted to concentration using an extinction coefficient at 280 nm of 1.4 for IgG [22].

Biotin-conjugated polyacrylamide (PAA)-sLe^x [23,24] (Glycotech; Rockville, MD) was conjugated to FITC using an EZ-Label™ FITC protein labeling kit from Pierce. A pre-measured amount of FITC dye (1 mg) was dissolved in dimethylformamide (DMF), which was then added to the unlabeled polymer at a 100-fold molar excess and incubated at room temperature for an hour. Excess free dye was removed with a 5 kDa MW cut-off Amicon (Millipore; Billerica, MA) tube.

All microbubbles used for this project were manufactured by Dr. A. Klibanov at the University of Virginia, Department of Medicine, Division of Cardiovascular Medicine. Briefly, microbubbles were manufactured by sonic dispersion of perfluorocarbon with PEG-dSPE (with a 40-mer length), biotin-PEG-dSPE (76-mer length) and phosphatidylcholine (Avanti Polar Lipids; Alabaster, AL). Excess materials, such as phospholipid fragments and unbound PEG, were

removed by serial centrifugal flotation at 160*g* for 5 min, taking advantage of the fact that microbubbles are buoyant in suspension. All microbubble samples were stored in sealed glass vials with a perfluorocarbon gas head-space to prevent microbubble deflation. Microbubbles were stable when stored at 4 °C for extended periods of time (months).

Unconjugated biotin bubbles were washed three to four times in a centrifuge at 160*g* for 5 min to remove deflated microbubbles and fragments. Microbubbles were counted with a CoulterMultisizer IIe (Beckman Coulter; Hialeah, FL), incubated with 3 μg/10^7 microbubbles of streptavidin (Sigma Chemical Co.; St. Louis, MO) for 10 min at room temperature, washed with degassed perfluorocarbon-saturated PBS (Gibco; Carlsbad, CA) twice and counted.

For flow cytometry experiments, streptavidin-coated microbubbles were conjugated with titrated amounts of either Alexa Fluor 647–biotin–MVCAM.A(429) or FITC–biotin–PAA-sLe^x for 10 min at room temperature and then washed to remove excess dye. Dual-targeted microbubbles with both sLe^x and Alexa Fluor 647–MVCAM.A(429) were sequentially incubated with the carbohydrate for 10 min and then the antibody for an additional 10 min prior to washing. Using sequential incubations for sLe^x and MVCAM.A(429), we were able to control the amount of each of these molecules that bound to microbubbles in a reproducible manner.

For flow chamber experiments, microbubbles were conjugated to the desired amounts of unlabeled biotinylated MVCAM.A(429) and/or sLe^x for dual- or single-targeted bubbles respectively. Since sialyl Lewis^x rolling/binding interactions are calcium dependent experiments in which microbubbles were targeted with sLe^x were supplemented with calcium chloride (0.9 mM) and magnesium chloride (1 mM) (Gibco). Briefly, 500 ml of DPBS was degassed under vacuum for 30 min prior to use and saturated with C_4F_{10} gas to ensure microbubble stability for the duration of the experiment. Dual-targeted microbubble formulations were prepared by adding, to streptavidin conjugated microbubbles, first sLe^x for 10 min at room temperature with perfluorocarbon gas head-space, then, MVCAM.A(429) for an additional 10 min. Microbubble samples were washed by centrifugal flotation to remove excess unbound ligands from the buffer. For single-targeted formulations of MVCAM.A(429) microbubbles, an initial 10 minute incubation step was performed with a non-binding carbohydrate polymer, $HOCH_2(HOCH)_4$-CHNH-PAA-Biotin (Glycotech).

2.4. Microbubble surface density characterization

Fluorescence intensity of microbubbles and Simply Quantum Cellular (SQC) calibration beads (Bangs Labs; Fishers, IN), conjugated with fluorescently-labeled mouse IgG mAbs was determined by flow cytometry (FACSCalibur, Becton Dickinson; Franklin Lakes, NJ). Controls to determine the amount of non-specific binding consisted of biotin microbubbles incubated with fluorescently-labeled antibodies without the streptavidin coupling component. All FACSCalibur settings for Alexa Fluor 647and FITC samples were kept constant between experiments.

FITC–sLe^x conjugated to the surface of microbubbles was measured using a spectrofluorometric assay [20]. FITC–sLe^x-conjugated microbubbles were sonicated in a water-bath sonicator twice for 30 min to remove the gas inside microbubbles and reduce turbidity of the sample, and were added to wells of a 96-well Costar plate (Corning, NY). A SPECTRAmax Gemini XS fluorescence plate reader (Molecular Devices; Sunnyvale, CA) was used to measure the fluorescence of each microbubble preparation at 485 nm excitation and 534 nm emission. Results were compared to a FITC–sLe^x standard curve. A standard curve was generated for each experiment by measuring the fluorescence intensity of known amounts of FITC–sLe^x with the fluorescence plate reader. Control microbubbles without fluorescent FITC were used to correct the results for residual sample turbidity.

2.5. Flow chamber experiments

A parallel plate flow chamber system (Glycotech; Rockville, MD) [20] was used to characterize microbubble attachment efficiency to substrates adsorbed with P-selectin.Fc, VCAM-1.Fc or both. The silicon gasket used for all experiments had a width of 2.5 mm and nominal thickness of 0.127 mm. The wall shear stress was adjusted to 1.5, 3 and 6 dyn/cm^2 by varying the flow rate of a syringe pump (Harvard Apparatus; Holliston, MA). The flow chamber was inverted in a custom-built mount to account for microbubble buoyancy and allow microbubbles to interact with the substrate surface. Well-mixed solutions of microbubbles diluted to $5*10^7$ bubbles/ml in degassed C_4F_{10}-saturated DPBS (prepared as previously described) with 0.1% bovine serum albumin (BSA) were introduced into the flow chamber by a syringe pump in withdraw mode to prevent microbubble destruction and allow mixing with a magnetic stir bar. All connections used were PE 60 (Becton Dickinson; Sparks, MD) tubing with an internal diameter of 0.76 mm. Dual- and single-targeted microbubbles were prepared and used on the same day. The flow chamber was assembled in a PBS bath to ensure that no air bubbles were introduced into the system.

Each flow chamber was imaged with a Zeiss Axioskop microscope equipped with a 40×/0.75 NA water immersion objective resulting in a field of view of 800 by 600 pixels or 296 by 222 μm. For each shear stress condition, a sequence of 405 tiff images were sampled at 8.96 frames per second (fps), corresponding to 45 s. A digital pco.1600 CCD camera (Cooke Corporation; Romulus, MI) was used to collect all data. The camera delay time was always set at 5 ms and the exposure time at 10 ms.

2.6. Data and statistical analysis

The resulting images were transferred to an analysis computer (quad-core Pentium IV Dell with 4 GB RAM) and converted to audio-video-interlaced (avi) sequence files in a Matlab routine. Adherent microbubbles and free-flowing microbubbles (appearing as dark, focused streaks crossing the field of view) were counted by hand with a cell counter and adherent microbubbles at the beginning of a video were subtracted as background. Microbubbles that remained stationary for longer than 5 s were considered to be adherent [24,25]. Stationary microbubbles were assessed by eye as microbubbles that moved less than ¼ their own diameter over 3 to 4 frames. Rychak et al. showed that microbubbles that attached to the substrate for 5 s remained bound for the duration of the experiment (5 min) [25]. Microbubble aggregates of less than three bubbles that were seen to attach were counted as one microbubble. Larger aggregates were not observed in these experiments. Occasionally, secondary interactions between adherent and flowing microbubbles led to their attachment downstream. These newly attached microbubbles were also taken into account as adherent. Transient interactions occasionally resulted in rolling interactions and were not counted. Adherent microbubbles were normalized by the free-flowing microbubble flux (i.e. bubbles available at the surface to bind). Microbubble adhesion efficiency was compared with a two-tailed Student *t*-test, $p<0.05$, considered significant. Error bars shown on graphs are the standard error of the mean (SEM).

3. Results

Perfluorocarbon-filled lipid-shelled microbubbles were coated with MVCAM.A(429), PAA-sLe^x or both for targeting to VCAM-1 or P-selectin respectively (Fig. 1). Flow chamber substrate site densities were measured at 0, 0.5, 1, 2, 4, 8, 16 and 30 ng/μl plating concentrations of VCAM-1.Fc or P-selectin.Fc, using radioactively labeled antibodies against VCAM-1 or P-selectin (Fig. 2). These measurements were compared against radioactively labeled isotype control antibodies (R3-34 IgG_1 for

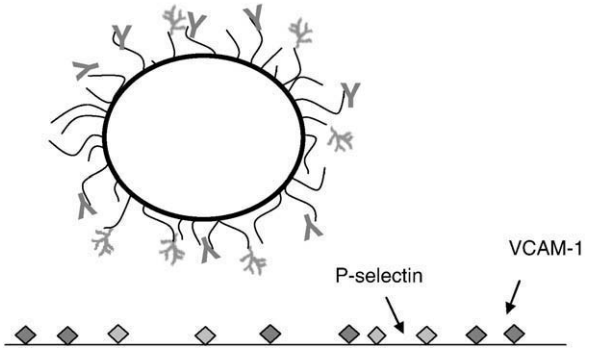

Fig. 1. Perfluorocarbon-filled microbubble targeted with MVCAM.A(429) against VCAM-1 (Y-shaped on bubble) and polymeric Sle^x (branch-shaped), which binds selectins. A biotin–streptavidin coupling system is used to graft biotinylated mAbs and carbohydrates on the PEG brush (black arms extending from microbubble surface) covering the phospholipid shell (thick, black circle) of ultrasound contrast agent microbubbles.

Rb40.34 and R35-95 IgG_{2a} for MVCAM.A(429)). As an additional control for non-specific binding and to test the cross-reactivity of the radioactive antibodies, substrates coated with P-selectin were probed with anti-VCAM-1 mAb and VCAM-1 dishes were probed with anti-P-selecting mAb. Both sets of controls show that binding of MVCAM.A(429) is specific to VCAM-1, while Rb40.34 specifically binds P-selectin. Results indicate that the coated substrate area saturated with VCAM-1 at approximately 1200 molecules/μm^2 (Fig. 2A), while P-selectin saturation is observed to occur at approximately 800 molecules/μm^2 (Fig. 2B).

Dually coated polystyrene dishes were coated with 50% VCAM-1 and 50% P-selectin and probed with either radioactive MVCAM.A (429) (Fig. 2C) or Rb40.34 (Fig. 2D). Protein adsorption for each of these molecules was found to be approximately 50 to 60% of that measured for their single coated counterparts at the same nominal plating concentrations. For flow chamber experiments, both VCAM-1 and P-selectin were coated at 7.5 ng/μl each, which is near saturation for both proteins.

Fig. 3 shows the number of MVCAM.A(429) molecules per microbubble. Mean fluorescence intensity as determined by flow cytometry increased with increasing MVCAM.A(429) concentration added to the microbubble preparations. Coating concentrations higher than 10 μg/10^7 microbubbles were not investigated because other investigators [26,27] found that this amount was sufficient to saturate the surface of microbubbles.

Dual-targeted microbubbles with titrated amounts of both sLe^x and Alexa Fluor 647-labeled MVCAM.A(429) were also sampled by flow cytometry. Microbubbles incubated with 0.5 μg/10^7 microbubbles of sLe^x and fluorescent MVCAM.A(429) at 0.1, 0.5, 1, 2.5 and 5 μg/10^7 microbubbles reached saturation at approximately 1 μg of antibody per 10^7 microbubbles (Fig. 4A). Experiments were then conducted on microbubbles with titrated sLe^x (0.1, 0.5, 1 and 2.5 μg/10^7) but with constant fluorescent MVCAM.A(429) at 1 μg/10^7 microbubbles (Fig. 4B). Based on these results, the formulation of dual-targeted microbubbles chosen for further flow chamber experiments was 0.5 μg of sLe^x and 1 μg of MVCAM.A(429) for 10^7 microbubbles. The number of PAA-sLe^x molecules attached to the surface of microbubble samples was determined by a spectrofluorometric assay with titrated amounts of FITC–sLe^x (0, 0.1, 0.25, 0.5 and

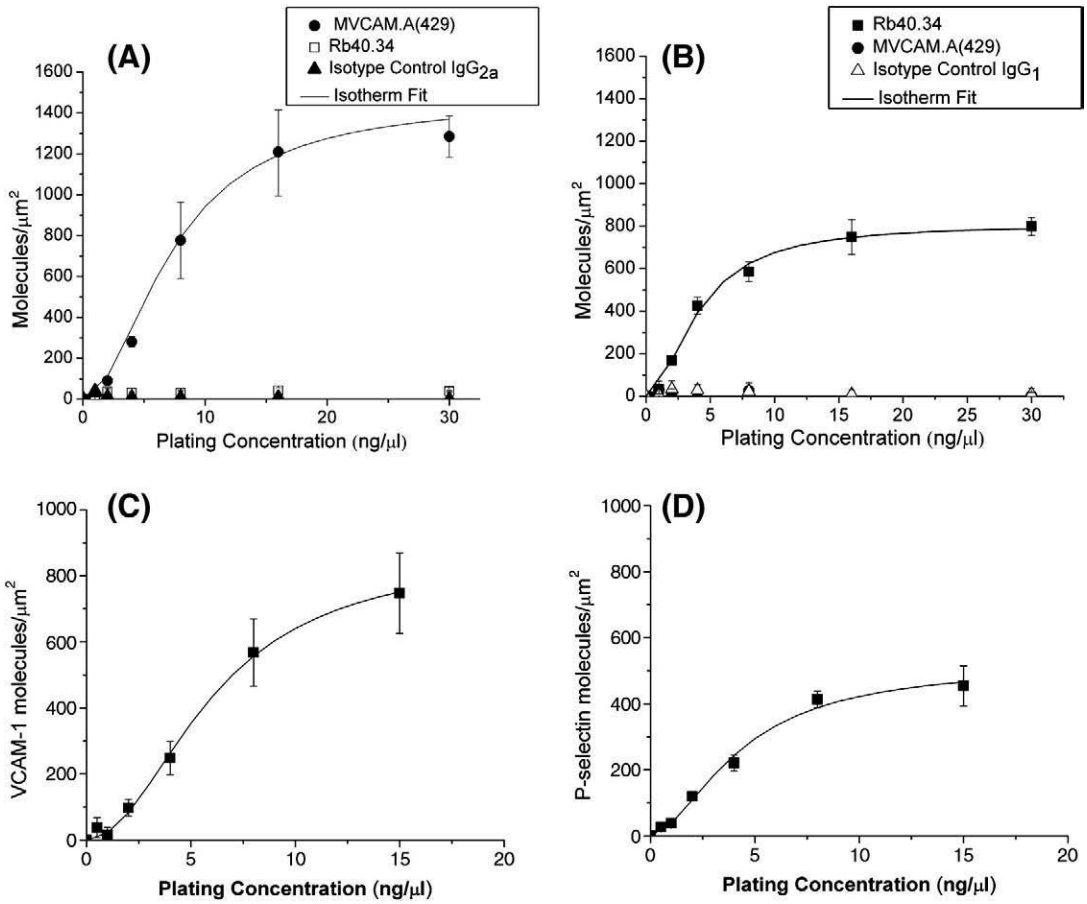

Fig. 2. Site density (molecules/μm^2) of VCAM-1 (A) and P-selectin (B) coated individually or together (dual substrates, C and D) on polystyrene flow chamber substrates. Results are measured in triplicate, ± SEM. Background radioactivity was subtracted from all data points.

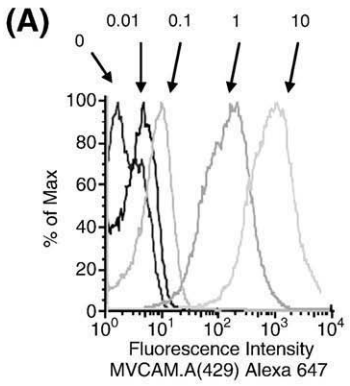

(B)

Coating Concentration ($\mu g/10^7$ microbubble)	Microbubble (MFI)	Targeted microbubbles (molecules/microbubble)	SEM
0 $\mu g/10^7$	107	0	169
0.01 $\mu g/10^7$	192	1,152	206
0.1 $\mu g/10^7$	365	12,898	424
1 $\mu g/10^7$	547	110,525	189
10 $\mu g/10^7$	632	296,179	257

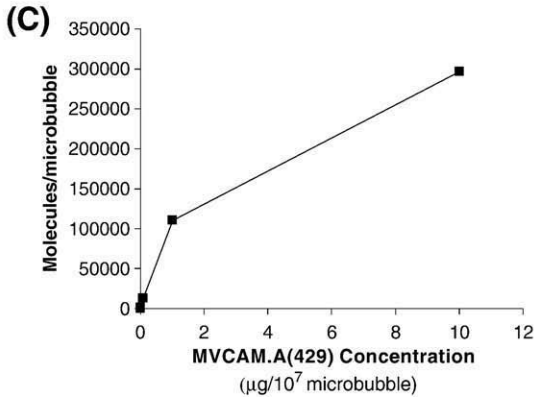

Fig. 3. Fluorescence intensity and number of molecules/microbubble based on FACSCalibur data of microbubbles conjugated with Alexa 647–MVCAM.A(429). (A) Fluorescence histograms of microbubbles conjugated with fluorescent antibody at the indicated concentrations ($\mu g/10^7$ microbubbles). Results from calibration beads were used to calculate the number of fluorescent molecules attached to the surface of microbubbles. (B) Table shows results of molecules/microbubble with respect to the fluorescent antibody concentration and what the microbubbles were incubated with. (C) MVCAM.A (429) site density per microbubble as a function of antibody concentration ($\mu g/10^7$ microbubbles). Background fluorescence values were subtracted from results; $n=4$, MFI — mean fluorescence intensity.

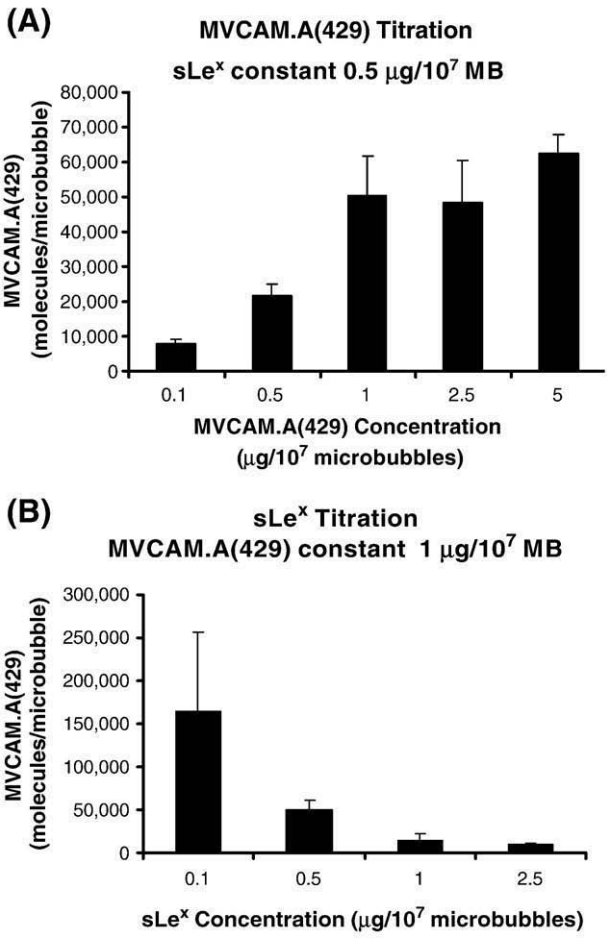

Fig. 4. MVCAM.A(429) site density as a function of MVCAM.A(429) concentration when microbubbles are incubated with the indicated concentrations (A) or as a function of PAA-sLe^x when microbubbles are incubated with a constant amount of MVCAM.A(429) (1 $\mu g/10^7$ microbubbles, B).

1 $\mu g/10^7$ microbubbles of FITC–sLe^x). FITC–sLe^x reached saturation at 0.5 $\mu g/10^7$ microbubbles (data not shown).

Dual-targeted microbubbles were made with 0.5 $\mu g/10^7$ of sLe^x and 1 $\mu g/10^7$ of MVCAM.A(429) based on the flow cytometry results for dual-targeted microbubbles and compared to single-targeted sLe^x microbubbles (0.5 $\mu g/10^7$ microbubbles) and MVCAM.A(429) (1 $\mu g/10^7$ microbubbles) bubbles (Fig. 5). The adhesion efficiency of microbubbles, defined as the ratio of bound to flowing microbubbles within the investigated region, was significantly higher for dual-targeted microbubbles at shear stresses of 3 and 6 dyn/cm^2 than for either single-targeted microbubble composition (Fig. 5).

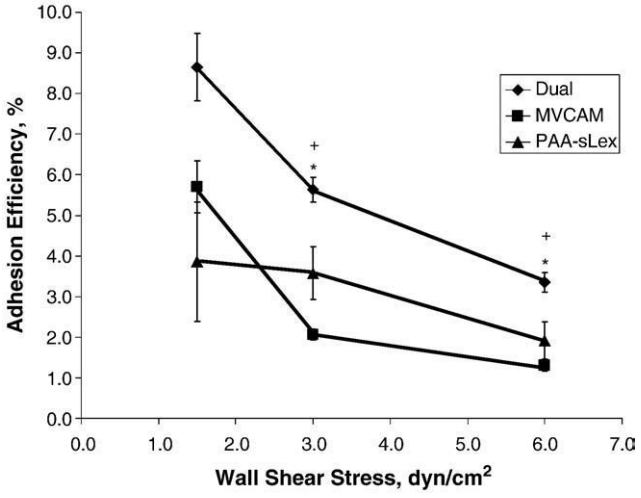

Fig. 5. Microbubble adhesion efficiency within a parallel plate flow chamber. Streptavidin microbubbles conjugated with 0.5 $\mu g/10^7$ microbubbles PAA-sLe^x for 10 min at room temperature and, then, 1 $\mu g/10^7$ microbubbles of MVCAM.A(429) for 10 min. Attachment efficiency (adherent microbubbles/all microbubbles passing field of view per 45 s) of dual, MVCAM.A(429)-targeted microbubbles and PAA-sLe^x microbubbles as a function of shear stress. "*", $p<0.05$ from sLe^x microbubbles. "+", $p<0.05$ from MVCAM.A(429) microbubbles. Error bars, SEM for $n=8$.

4. Discussion

The focus of this investigation was directed towards three critical parameters: the surface coverage of targeting molecules on single- and dual-targeted microbubbles, the molecular composition of the flow chamber substrates and the effects of wall shear stress on the

accumulation efficiency of single- and dual-targeted microbubbles. At well-defined site density parameters for both microbubbles and substrates, we demonstrated that dual-targeted microbubbles show increased adhesion efficiency in fluid shear environments in a parallel plate flow chamber.

Several investigators have previously attempted to characterize various aspects of microbubble surface coverage and shear stress response behavior, but to date no complete characterization has been accomplished. In 2001, Lindner et al. [26] used flow cytometry and a FITC-labeled antibody against P-selectin to determine its saturating site density on the surface of microbubbles in an attempt to maximize microbubble attachment in vivo. Weller et al. used similar methods for microbubbles targeted against ICAM-1 and showed how microbubble behavior was affected by shear rate [28]. A prior study from our group characterized targeted microbubbles with respect to P-selectin site density on the flow chamber substrate and the site density of P-selectin antibody on microbubbles [20].

Dual-targeted microbubbles (anti-ICAM-1 and sLe^x) were first used by Weller et al. on activated endothelial cells as the targeting substrate [29]. This group used flow cytometry to measure the relative amounts of molecules on the microbubble and determine the expression level of pro-inflammatory molecules on the substrate endothelial cells. These microbubbles were probed with secondary antibodies against each of these molecules. With these methods, they estimated that their single-targeted microbubbles had $250{,}000 \pm 50{,}000$ molecules of sLe^x per microbubble and $60{,}000 \pm 5000$ molecules of anti-ICAM-1 on their surface. Dual-targeted microbubbles were manufactured to have approximately 50% of sLe^x and of ICAM-1 antibody.

This is the first study showing site density measurements of P-selectin, VCAM-1 and dual composition substrates. Although radioactive techniques [30–33] for site density measurements are well established, these methods have not previously been used for microbubble adhesion assays. For single-targeted substrates, saturation on the substrate is achieved at 15 ng/μl of protein, corresponding to 800 and 1200 molecules/μm^2 for P-selectin and VCAM-1, respectively. At the lower portion of these binding isotherms, between 0 and 2.5 ng/μl, both molecules seem to bind the substrate with low affinity until a certain concentration is reached. This type of behavior is called cooperative binding and has been investigated by Monod [34] in a model that explains that molecules exhibit a low affinity state if low amounts of ligand are present. A switch can then occur towards a higher affinity state as the bound ligand increases [34]. Differences between the binding curves for these molecules may be accounted for by the fact that the Fc binding region (with which the protein binds the substrate) for each of these molecules may have different properties. Additionally, these molecules most likely bind the substrates in random orientations so that the active site for some of the molecules may actually be facing the substrate, preventing it from binding to the antibody. One of the advantages of using the radioactively labeled antibody to probe the substrate composition is that only molecules with active sites available to bind the antibody are detected so that the site density measurements obtained are "functional" site densities. Translating this concept to the flow chamber experiments, this characterization provides a reliable measure of how many molecules are actually available to bind flowing microbubbles rather than a bulk measurement of total site density, including molecules that may be blocked from binding due to orientation. The results obtained with these methods for P-selectin coated substrates probed with Rb40.34 extend the findings obtained by Takalkar et al. [20] to higher site densities and dual substrates. The P-selectin site density adsorption isotherm they obtained by a europium–streptavidin assay [20] corresponds to the lower range of the binding isotherm presented in Fig. 2.

In a study of human neutrophil migration under shear flow in a parallel plate flow chamber, Hammer et al. [35] investigated E-selectin alone and in combination with ICAM-1 or PECAM-1 (CD31). All adhesion molecules were used as Fc fusion proteins and adsorbed to polystyrene dishes in 200 μl binding buffer at pH 9.2 and blocked with 0.5% Tween. E-selectin-Fc was coated at 0.1 and 1 μg/ml with and without 4 μg/ml ICAM-1-Fc or 0.5, 1 or 4 μg/ml PECAM-1-Fc. Although site densities were not reported [35], resulting site densities can be estimated to range between 50 and 200 molecules per μm^2 based on our present data. At these concentrations and site densities, the addition of a second molecular species is expected to have little impact on the adsorption of the other molecular species such that site densities for E-selectin, ICAM-1 and PECAM-1 can be treated as quasi-independent.

Haun and Hammer [36] analyzed attachment of 210 nm beads coated with a mAb to ICAM-1 to an ICAM-1-Fc substrate at wall shear rates between 100 and 1000 s^{-1}. Their approach differs from ours in that only a single substrate (ICAM-1) is used, and only a single ligand (Anti-ICAM-1) is used for targeting, that the particles are about 10 times smaller in linear dimension, and that the site densities achieved on the substrate remain far from saturation. This is because ICAM-1-Fc was immobilized at a fixed total concentration of 100 nM, of which 1.25% to 100% was active ICAM-1-Fc, resulting in maximum site densities of 134 sites per μm^2. Although the binding curve shown in their Fig. 2B is not drawn to scale, it is suggestive of the concaveness we found for binding of low concentrations of VCAM-1-Fc and P-selectin-Fc. Haun and Hammer might have achieved higher site densities if the concentration of ICAM-1-Fc had been increased. Alternatively, it is possible that the amount of glass-adsorbed protein G may have become limiting, although this is less likely in view of the high concentration of protein G used (0.7 ml of 100 μg/ml). These authors suggest that both protein G and ICAM-1-Fc were at saturating concentrations, but provide no evidence for this assertion. Our data would suggest that saturation for directly adsorbed Fc fusion proteins is reached at about 30 μg/ml, which corresponds to about 200 μM, equal to 2000 times the ICAM-1-Fc concentration used in the previous study [36]. Over the site density range between 8 and 134 molecules per μm^2, Haun and Hammer found linear accumulation of nanobeads over time, consistent with our earlier results with microbubbles attaching to a single molecular substrate [20].

Measurements of the surface coverage of molecules conjugated to the surface of microbubbles were accomplished using fluorescently-labeled molecules and flow cytometry [25]. Fluorescence intensity values for titration curves were compared to those of calibration beads conjugated with the same antibody and showed that MVCAM.A(429)-conjugated microbubbles reach coverage near the saturation region (10 μg/10^7 microbubbles) at approximately 300,000 molecules/microbubble. These results of molecule surface coverage of antibodies are consistent with previously obtained results with similar methods for microbubbles coated with fluorescent RB40.34 (against P-selectin) with a ligand density of 300,000 molecules/microbubble [26].

Conjugating microbubbles at even low concentrations of PAA-sLe^x takes up many binding sites and impairs subsequent binding of MVCAM.A(429) to the microbubble surface. For this reason, dual-targeted microbubbles were produced by sequential conjugation with sLe^x and then MVCAM.A(429), which resulted in a high level of reproducibility with respect to microbubble surface composition. Based on flow cytometry results, the formulation of dual-targeted microbubbles that was pursued for flow chamber experiments consisted of 0.5 μg of sLe^x and 1 μg of MVCAM.A(429) per 10^7 microbubbles.

Flow chamber experiments were conducted at shear stresses of 1.5, 3 and 6 dyn/cm^2. At the low shear stress setting (1.5 dyn/cm^2), all microbubble formulations, single and dual, performed similarly. At higher shear stresses, the adhesion efficiency of microbubbles conjugated with the antibody rapidly decreased in a shear stress dependent manner. Dual microbubbles performed significantly better at 3 and 6 dyn/cm^2. This is similar to previous observations obtained with dual-targeted polystyrene beads [37].

Decuzzi and Ferrari [38] provide a very interesting theoretical treatment of nanoparticle adhesion to a single class of receptors. Their work suggests that for a given set of non-specific interaction parameters, wall shear stress, bond compliance and binding affinity, the probability of

adhesion only depends on the ratio of ligands on the nanoparticle to receptors on the endothelium or stationary substrate. Although this approach provides a very appealing framework for developing design maps, no experimental data are provided that would support the proposed model in detail. From our present data, we can estimate that, based on the larger particle size of microbubbles used for these experiments, a larger number of ligands is required for the attractive forces needed for firm adhesion to take place in high shear stress flow fields, assuming a 50% probability of adhesion (as shown in their Fig. 5 [38]).

With the objective of targeting inflamed vasculature, antibodies against several of the relevant adhesion molecules are commercially available. These molecules can be conjugated to microbubbles and provide high specificity against their target ligands for pre-clinical work. Microbubbles conjugated to humanized or fully human antibodies may be useful for diagnostic tests in patients. In addition to the in vitro characterization experiments and in vivo mouse disease models, it will be necessary to acquire suitable human antibodies to translate this technology to the clinical setting. SLe^x is a molecule that has good targeting potential to P-selectin, because it is found as a post-translational modification on the P-selectin ligand PSGL-1 that mediates leukocyte rolling in vivo [16]. Additionally, the fast binding kinetics of this molecule with its ligand nicely complements the slow detachment kinetics of the antibody targeting system. Another advantage is that for eventual translation to clinical applications, this type of synthetic carbohydrate molecule can be used in humans because it is a natural blood group antigen. However, the biotin–streptavidin bridge needs to be replaced. While this coupling technique provides flexibility, it cannot be used in a clinical setting. Alternative methods exist for direct covalent conjugation of ligands to the surface of the microbubbles [39].

An important consideration for translation of targeted microbubbles from research development to the clinical setting is their size distribution. While sonic dispersion techniques produce high numbers of microbubbles, the population has a large variation in microbubble size (as do commercially available microbubbles). The resonant frequency of a microbubble varies with its size so a large variation in size also produces a large variation in resonant frequency and ultrasound image quality, which is due to the limited bandwidth frequency of the ultrasound transducer. Additionally, while larger microbubbles have more surface area, allowing for more binding sites, they also will experience higher drag forces once they are bound. Smaller microbubbles need to have the proper balance of binding sites, allowing them to bind to the target substrate and remain bound. Monodisperse microbubbles can be manufactured with microfluidics methods [40]. Currently, these production techniques yield only small amounts of microbubbles. The size distribution of the microbubbles used for experiments reported here was narrowed to a range between approximately 1.5 and 3 μm (mean diameter is 2.3 μm) using serial centrifugation/flotation techniques to separate microbubbles by size, ensuring a fairly narrow size distribution.

Targeted microbubbles can be tailored to detect plaques at early stages of development, leading to treatment of the diseased area before a severe cardiac event takes place. It is possible that, eventually, targeted microbubbles will be available to successfully detect vascular disease and even vulnerable plaques. The use of these contrast agents may even be coupled with therapeutic drugs as a drug delivery vehicle to diseased tissue, thus bypassing more invasive treatments [41]. The work presented here provides useful and thorough methods for a full characterization of single- and dual-targeted microbubbles in terms of ligand surface coverage, receptor molecule site densities on substrates and adhesion efficiency under flow. Flow chamber experiments show that dual-targeted microbubbles perform significantly better than their single-targeted counterparts at high shear stress levels in a parallel plate flow chamber, suggesting that such contrast agents may be suitable for molecular imaging in high-flow vessels.

References

[1] W. Rosamond, K. Flegal, K. Furie, A. Go, K. Greenlund, N. Haase, S.M. Hailpern, M. Ho, V. Howard, B. Kissela, S. Kittner, D. Lloyd-Jones, M. McDermott, J. Meigs, C. Moy, G. Nichol, C. O'Donnell, V. Roger, P. Sorlie, J. Steinberger, T. Thom, M. Wilson, Y. Hong, Heart disease and stroke statistics—2008 update: a report from the American Heart Association Statistics Committee and Stroke Statistics Subcommittee, Circulation 117 (4) (2008) e25–146.

[2] E. Galkina, K. Ley, Vascular adhesion molecules in atherosclerosis, Arterioscler. Thromb. Vasc. Biol. 27 (11) (2007) 2292–2301.

[3] M.J. Hickey, S. Kanwar, D.M. McCafferty, D.N. Granger, M.J. Eppihimer, P. Kubes, Varying roles of E-selectin and P-selectin in different microvascular beds in response to antigen, J. Immunol. 162 (2) (1999) 1137–1143.

[4] E.Y. Park, M.J. Smith, E.S. Stropp, K.R. Snapp, J.A. DiVietro, W.F. Walker, D.W. Schmidtke, S.L. Diamond, M.B. Lawrence, Comparison of PSGL-1 microbead and neutrophil rolling: microvillus elongation stabilizes P-selectin bond clusters, Biophys. J. 82 (4) (2002) 1835–1847.

[5] K. Ley, C. Laudanna, M.I. Cybulsky, S. Nourshargh, Getting to the site of inflammation: the leukocyte adhesion cascade updated, Nat. Rev. Immunol. 7 (9) (2007) 678–689.

[6] H.C. Stary, A.B. Chandler, R.E. Dinsmore, V. Fuster, S. Glagov, W. Insull Jr., M.E. Rosenfeld, C.J. Schwartz, W.D. Wagner, R.W. Wissler, A definition of advanced types of atherosclerotic lesions and a histological classification of atherosclerosis. A report from the Committee on Vascular Lesions of the Council on Arteriosclerosis, American Heart Association, Arterioscler. Thromb. Vasc. Biol. 15 (9) (1995) 1512–1531.

[7] H.C. Stary, A.B. Chandler, S. Glagov, J.R. Guyton, W. Insull Jr., M.E. Rosenfeld, S.A. Schaffer, C.J. Schwartz, W.D. Wagner, R.W. Wissler, A definition of initial, fatty streak, and intermediate lesions of atherosclerosis. A report from the Committee on Vascular Lesions of the Council on Arteriosclerosis, American Heart Association, Circulation 89 (5) (1994) 2462–2478.

[8] P. Libby, P.M. Ridker, A. Maseri, Inflammation and atherosclerosis, Circulation 105 (9) (2002) 1135–1143 (2002/3/5).

[9] M. Aikawa, P. Libby, The vulnerable atherosclerotic plaque: pathogenesis and therapeutic approach, Cardiovasc. Pathol. 13 (3) (2004) 125–138.

[10] P.J. Cassidy, G.K. Radda, Molecular imaging perspectives, J. R. Soc. Interface 2 (3) (2005) 133–144.

[11] T.F. Massoud, S.S. Gambhir, Molecular imaging in living subjects: seeing fundamental biological processes in a new light, Genes Dev. 17 (5) (2003) 545–580.

[12] D. Cosgrove, Ultrasound contrast agents: an overview, Eur. J. Radiol. 60 (3) (2006) 324–330.

[13] L.W. Dobrucki, A.J. Sinusas, Cardiovascular molecular imaging, Semin. Nucl. Med. 35 (1) (2005) 73–81.

[14] C.Z. Behm, J.R. Lindner, Cellular and molecular imaging with targeted contrast ultrasound, Ultrasound Q. 22 (1) (2006) 67–72.

[15] B.A. Kaufmann, J.R. Lindner, Molecular imaging with targeted contrast ultrasound, Curr. Opin. Biotechnol. 18 (1) (2007) 11–16.

[16] T. Tamatani, M. Suematsu, K. Tezuka, N. Hanzawa, T. Tsuji, Y. Ishimura, R. Kannagi, S. Toyoshima, M. Homma, Recognition of consensus CHO structure in ligands for selectins by novel antibody against sialyl Lewis X, Am. J. Physiol. 269 (4 Pt 2) (1995) H1282–H1287.

[17] M.E. Beauharnois, K.C. Lindquist, D. Marathe, P. Vanderslice, J. Xia, K.L. Matta, S. Neelamegham, Affinity and kinetics of sialyl Lewis-X and core-2 based oligosaccharides binding to L- and P-selectin, Biochemistry 44 (27) (2005) 9507–9519.

[18] T. Kinashi, T.A. Springer, Adhesion molecules in hematopoietic cells, Blood Cells 20 (1) (1994) 25–44.

[19] R. Bosse, D. Vestweber, Only simultaneous blocking of the L- and P-selectin completely inhibits neutrophil migration into mouse peritoneum, Eur. J. Immunol. 24 (12) (1994) 3019–3024.

[20] A.M. Takalkar, A.L. Klibanov, J.J. Rychak, J.R. Lindner, K. Ley, Binding and detachment dynamics of microbubbles targeted to P-selectin under controlled shear flow, J. Control. Release 96 (3) (2004) 473–482.

[21] L.C.L. Aquino, E.A. Miranda, Adsorption of human immunoglobulin G onto ethacrylate and histidine-linked methacrylate, Braz. J. Chem. Eng. 20 (3) (2003) 251–262.

[22] G.C. Howard, D.R. Bethell, Basic Methods in Antibody Production and Characterization, CRC Press, Boca Raton, 2001.

[23] A.L. Klibanov, J.J. Rychak, W.C. Yang, S. Alikhani, B. Li, S. Acton, J.R. Lindner, K. Ley, S. Kaul, Targeted ultrasound contrast agent for molecular imaging of inflammation in high-shear flow, Contrast Media Mol. Imaging 1 (6) (2006) 259–266.

[24] J.J. Rychak, B. Li, S.T. Acton, A. Leppanen, R.D. Cummings, K. Ley, A.L. Klibanov, Selectin ligands promote ultrasound contrast agent adhesion under shear flow, Mol. Pharmacol. 3 (5) (2006) 516–524.

[25] J.J. Rychak, J.R. Lindner, K. Ley, A.L. Klibanov, Deformable gas-filled microbubbles targeted to P-selectin, J. Control. Release 114 (3) (2006) 288–299.

[26] J.R. Lindner, J. Song, J. Christiansen, A.L. Klibanov, F. Xu, K. Ley, Ultrasound assessment of inflammation and renal tissue injury with microbubbles targeted to P-selectin, Circulation 104 (17) (2001) 2107–2112.

[27] C. Bachmann, A.L. Klibanov, T.S. Olson, J.R. Sonnenschein, J. Rivera-Nieves, F. Cominelli, K.F. Ley, J.R. Lindner, T.T. Pizarro, Targeting mucosal addressin cellular adhesion molecule (MAdCAM)-1 to noninvasively image experimental Crohn's disease, Gastroenterology 130 (1) (2006) 8–16.

[28] G.E. Weller, F.S. Villanueva, A.L. Klibanov, W.R. Wagner, Modulating targeted adhesion of an ultrasound contrast agent to dysfunctional endothelium, Ann. Biomed. Eng. 30 (8) (2002) 1012–1019.

[29] G.E. Weller, F.S. Villanueva, E.M. Tom, W.R. Wagner, Targeted ultrasound contrast agents: in vitro assessment of endothelial dysfunction and multi-targeting to ICAM-1 and sialyl Lewisx, Biotechnol. Bioeng. 92 (6) (2005) 780–788.

[30] M.J. Eppihimer, J. Russell, R. Langley, G. Vallien, D.C. Anderson, D.N. Granger, Differential expression of platelet-endothelial cell adhesion molecule-1 (PECAM-1) in murine tissues, Microcirculation 5 (2–3) (1998) 179–188.
[31] M.J. Eppihimer, B. Wolitzky, D.C. Anderson, M.A. Labow, D.N. Granger, Heterogeneity of expression of E- and P-selectins in vivo, Circ. Res. 79 (3) (1996) 560–569.
[32] M.L. Dustin, T.A. Springer, Lymphocyte function-associated antigen-1 (LFA-1) interaction with intercellular adhesion molecule-1 (ICAM-1) is one of at least three mechanisms for lymphocyte adhesion to cultured endothelial cells, J. Cell Biol. 107 (1) (1988) 321–331.
[33] M.B. Lawrence, T.A. Springer, Leukocytes roll on a selectin at physiologic flow rates: distinction from and prerequisite for adhesion through integrins, Cell 65 (5) (1991) 859–873.
[34] J. Monod, J. Wyman, J.P. Changeux, On the nature of allosteric transitions: a plausible model, J. Mol. Biol. 12 (1965) 88–118.
[35] L.A. Smith, H. Aranda-Espinoza, J.B. Haun, D.A. Hammer, Interplay between shear stress and adhesion on neutrophil locomotion, Biophys. J. 92 (2) (2007) 632–640.
[36] J.B. Haun, D.A. Hammer, Quantifying nanoparticle adhesion mediated by specific molecular interactions, Langmuir 24 (16) (2008) 8821–8832.
[37] A.O. Eniola, P.J. Willcox, D.A. Hammer, Interplay between rolling and firm adhesion elucidated with a cell-free system engineered with two distinct receptor-ligand pairs, Biophys. J. 85 (4) (2003) 2720–2731.
[38] P. Decuzzi, M. Ferrari, Design maps for nanoparticles targeting the diseased microvasculature, Biomaterials 29 (3) (2008) 377–384.
[39] A.L. Klibanov, M.S. Hughes, F.S. Villanueva, R.J. Jankowski, W.R. Wagner, J.K. Wojdyla, J.H. Wible, G.H. Brandenburger, Targeting and ultrasound imaging of microbubble-based contrast agents, Magma 8 (3) (1999) 177–184.
[40] E. Talu, K. Hettiarachchi, R.L. Powell, A.P. Lee, P.A. Dayton, M.L. Longo, Maintaining monodispersity in a microbubble population formed by flow-focusing, Langmuir 24 (5) (2008) 1745–1749.
[41] A.L. Klibanov, Microbubble contrast agents: targeted ultrasound imaging and ultrasound-assisted drug-delivery applications, Invest. Radiol. 41 (3) (2006) 354–362.